

RESEARCH ARTICLE

10.1002/2017JB014966

Key Points:

- We develop an earthquake catalog using the Cascadia Initiative ocean bottom seismometer data set for the entire Cascadia subduction zone
- Subduction zone and Juan de Fuca plate seismicity increases from north to south, with distinct increase in seismicity south of 46°N
- Seismicity varies with incoming plate smoothness and hydration, tied to observed trends in intraplate deformation and underthrust sediment

Supporting Information:

- Supporting Information S1
- Data Set S1
- Data Set S2
- Data Set S3
- Data Set S4
- Data Set S5

Correspondence to:

I. Stone,
ipstone@uw.edu

Citation:

Stone, I., Vidale, J. E., Han, S., & Roland, E. (2018). Catalog of offshore seismicity in Cascadia: Insights into the regional distribution of microseismicity and its relation to subduction processes. *Journal of Geophysical Research: Solid Earth*, 123, 641–652. <https://doi.org/10.1002/2017JB014966>

Received 11 SEP 2017

Accepted 5 JAN 2018

Accepted article online 11 JAN 2018

Published online 29 JAN 2018

Catalog of Offshore Seismicity in Cascadia: Insights Into the Regional Distribution of Microseismicity and its Relation to Subduction Processes

Ian Stone¹ , John E. Vidale², Shuoshuo Han³ , and Emily Roland⁴

¹Department of Earth and Space Sciences, University of Washington, Seattle, WA, USA, ²Department of Earth Sciences, University of Southern California, Los Angeles, CA, USA, ³Institute for Geophysics, University of Texas at Austin, Austin, TX, USA, ⁴Department of Oceanography, University of Washington, Seattle, WA, USA

Abstract We present a catalog of offshore seismicity generated from Cascadia Initiative (CI) ocean-bottom seismometer data. Earthquakes were detected within the CI data using a short-time-average/long-time-average trigger and located using 1-D velocity models developed from seismic reflection/refraction surveys. The catalog, which contains 271 earthquakes with magnitude 0.4–4.0 along the coasts of Vancouver Island, Washington, Oregon, and Northern California, spans all 4 years of the ocean bottom seismometer deployment and shows distinct along-strike variations in seismicity consistent with structural observations from recent active source seismic reflection/refraction studies. Seismicity is sparse off Vancouver Island and Washington (49°N–46°N) but increases off northern and central Oregon, corresponding to a roughened, more deformed subducting slab. Widespread earthquakes are observed at near-interface depths between 46°N and 45°N, though an increase in underthrust sediment thickness between 45°N and 43°N likely restricts seismicity to scattered asperities on the plate interface. South of 43°N, where both the overriding and subducting plates are severely deformed approaching the Mendocino triple junction, seismicity is abundant. We locate an additional 440 events in the Juan de Fuca plate seaward of the deformation front. The higher seismicity south of 46°N is consistent with more extensive intraplate deformation. Along with the complex stress field induced by the Mendocino triple junction, our observations imply that the smoothness and degree of hydration of the incoming plate, which are linked to the amount of underthrust sediment and extent of intraplate deformation, are major contributing factors to the distribution of microseismicity in the Cascadia subduction zone.

1. Introduction

The Cascadia subduction zone (CSZ), located off the coast of northwestern North America, facilitates a continent-scale collision between the Juan de Fuca (JdF) and North American tectonic plates. Here the JdF, which can be subset into a central primary plate, flanked to the north and south by the smaller Explorer and Gorda plates (Dziak et al., 2011; Gulick et al., 2001; Hyndman, Riddiough, & Herzer, 1979; Wilson, 1993), thrusts northeastwardly at 30–45 mm/yr (DeMets et al., 2010) into the upper mantle beneath North America. This collision creates a thousand-kilometer-long “megathrust” fault, which extends from the Queen Charlotte triple junction off Vancouver Island to the Mendocino triple junction off California. An extensive regional paleoseismic record indicates that the CSZ has hosted dozens of megathrust earthquakes in the past, with $M8+$ events occurring at ~250 year intervals, and ~ $M9$, full-margin events at ~500 year intervals (Goldfinger, Nelson, & Johnson, 2003; Goldfinger et al., 2012). The last such $M8+$ event in Cascadia happened in the year 1700, when a $M \sim 9$ event ruptured the full length of the subduction zone (Satake et al., 2003), and the only other historically recorded major event was the 1992 $M7.2$ Petrolia earthquake, which occurred just north of the Mendocino triple junction (Oppenheimer et al., 1993). Observations of present-day microseismicity along the margin are sparse, and only a handful of these events are believed to have occurred on the megathrust itself. While the CSZ’s quiescence may be related to relatively low rates of convergence and near-total locking on the plate interface (Wang & Tréhu, 2016), the paucity of observed events may be partially attributed to difficulty in monitoring.

Regional seismic networks, like the Pacific Northwest Seismic Network (PNSN), the Northern California Seismic Network (NCSN), the Canadian National Seismograph Network (CNSN), and the USArray

transportable array deployment, have provided the majority of our seismic observations of the CSZ. Despite covering an extensive geographic area, these networks are almost exclusively based on land. Because the CSZ's seismogenic zone is primarily offshore (Hyndman & Wang, 1995; McCaffrey et al., 2013; Schmalzle et al., 2014), seismic records of offshore events can be noisy with large azimuthal gaps, and smaller earthquakes are often missed altogether. Further, the velocity models used by the networks for locating offshore events have been necessarily simplified, failing to account for the complex source-to-receiver raypaths and lateral heterogeneities associated with the plate interface. As a result, significant location errors have been documented in some offshore event records (Tréhu, Braunmiller, & Davis, 2015; Tréhu, Braunmiller, & Nabelek, 2008; Williams et al., 2011). This implies that areas along the subduction zone with sparse, azimuthally restricted coverage and poor velocity characterization likely have severely biased earthquake locations.

Considering the disadvantages of using land-based seismic networks to monitor the subduction zone, offshore recordings of earthquakes are extremely valuable for determining more precise seismicity rates and earthquake locations. Offshore seismometer arrays are closer to the megathrust while also having source-to-receiver paths that are simpler than those associated with land-based networks. However, deploying and maintaining ocean bottom seismometers (OBSs) or cabled arrays is difficult both technically and logistically, and until recently, only a handful of studies utilizing OBS networks had been conducted on the CSZ.

Dziak et al. (2011) reviewed hydroacoustic data from 1991 to 2008 recorded on the U.S. Navy's submarine Sound Surveillance System (SOSUS) across the entire JdF and the CSZ. This work, which analyzed earthquake T-phases propagating through the North Pacific Ocean, cataloged over 45,000 earthquakes within and along the margins of the JdF. While the majority of these events were associated with spreading ridges and transform faults on the west and south edges of the JdF, many were located in the interior of the plate as well, with the highest rates of seismicity south of 46°N. Several hundred events were also recorded near the subduction zone.

Oregon State University deployed a 16-station short-period array of OBS off the coast of Newport, OR (~44.5°N), from September 2007 to July 2009 to monitor persistent swarm activity (Tréhu, Blakely, & Williams, 2012; Williams et al., 2011). These observations confirmed that there is seismic activity occurring directly on the plate interface. Further, these studies demonstrated that the PNSN was systematically overestimating the depth of offshore events. In 2010, the Seafloor Earthquake Array Japan-Canada Cascadia Experiment (Sea-Jade) collected continuous seismic data off the coast of Vancouver Island with a dense (~20 km spacing) array positioned directly over the CSZ (Scherwath et al., 2011). Although only deployed for 3 months, this array detected over 1,200 earthquakes, most of which were concentrated along the Nootka fault zone and in the fore arc of the overriding plate (Obana et al., 2015).

In each of these studies, the use of OBS deployments and velocity models appropriate for offshore geologic structure provided more detailed, accurate, and complete observations than those from regional land-based networks alone. The success of such projects provided an impetus for pursuing significantly larger deployments offshore.

Subsequently, the Cascadia Initiative (CI) was developed and implemented. The CI was a 4 year, community-organized OBS experiment that spanned the entirety of the CSZ, as well as most of the JdF (Toomey et al., 2014). It was the largest deployment of OBS in the region to date, and it vastly improved regional seismometer coverage. In this study, we present a catalog of seismicity developed from CI records, focusing primarily on earthquakes with epicenters in and adjacent to the CSZ. Our primary objective was to develop a standard seismic catalog that utilized near-source, offshore stations associated with the CI, potentially capable of detecting and determining improved locations for events associated with the CSZ's seismogenic zone. Further, we sought to characterize along-strike variations in interplate slip behaviors and intraplate deformation using trends in observed seismicity. Earthquakes were detected using a short-time-average/long-time-average (STA/LTA) trigger and located using a combination of 1-D velocity models developed from active source seismic surveys along the CSZ (Flueh et al., 1998; Gerdomeo et al., 2000). The results show a higher rate of seismicity in the subduction zone than was observed from land-based networks at the time of deployment. Further, the along-strike pattern of earthquake distribution supports observations that there are geologically and structurally distinct sections of the JdF that may affect seismic behavior in the subduction zone.

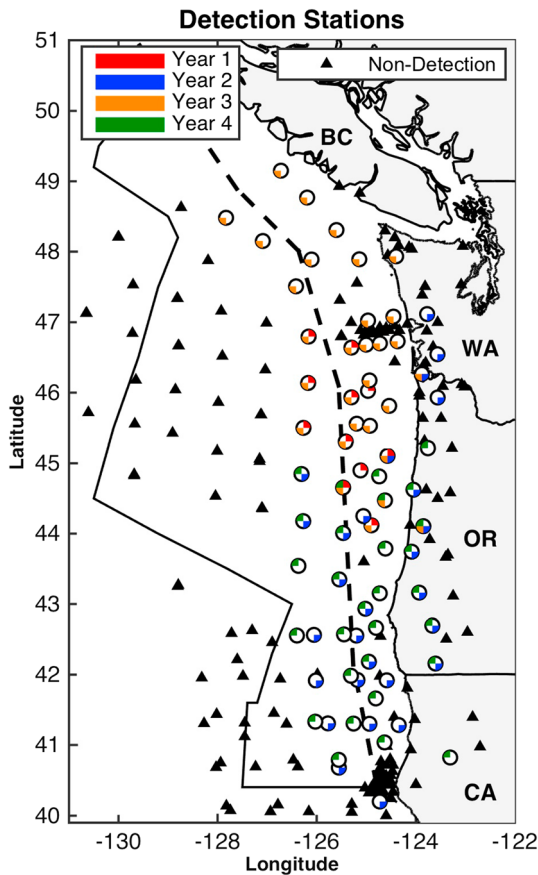


Figure 1. Cascadia Initiative (CI) OBS locations (offshore) and regional land-based seismometers. OBS and land stations used in earthquake detection are circles; colored quarters correspond to the year(s) the site was used for detection. Other CI OBS and land stations used in location but not detection are black triangles. The dashed line shows the location of the Cascadia deformation front, the western extent of the Cascadia subduction zone.

2. Data and Methods

The Cascadia Initiative was an National Science Foundation-supported, onshore/offshore seismic and geodetic experiment developed to increase observational coverage of the CSZ and the JdF. During this experiment, an OBS array was deployed off the coasts of Vancouver Island, Washington, Oregon, and Northern California. The array was emplaced in alternating northern and southern sections between 2011 and 2015, with each deployment consisting of 60–70 stations recording for approximately 10 months at a time. Station spacing varied depending on location, with stations on the JdF in a regular 70 km grid, and nearshore stations in a less regular ~50 km grid. There were also two dense arrays located on the continental shelf off Cape Mendocino, CA, and Grays Harbor, WA. The OBS recorded continuous broadband seismic time series at sampling rates of 50, 100, or 125 sps, depending on the instrument and deploying institution.

We selected stations to use in the detection based on their proximity to the subduction zone, their geometry relative to other stations, and by the quality of the data they produced (Figure 1). These data were supplemented with records from EarthScope transportable array stations on land, as well as records from regional land-based seismic networks. To begin, we searched for earthquakes sorting STA/LTA ratios on vertical traces (years 1–4) and horizontal traces (years 2–4) filtered between 3 and 15 Hz. To be considered a detection, the amplitude of the ratio needed to exceed a threshold value for a given duration of time. We identified optimal threshold values by first inspecting offshore events recorded by the PNSN during the time of the CI deployment. Upon finding a range of values that maximized the detection of known events, we applied the values to several week-long portions of the CI data, ultimately choosing a single set of values to apply to an entire year. The chosen STA/LTA and threshold values are shown in Table 1.

were visually inspected for validity. For detections to be flagged as an event, association of detections on at least three adjacent stations was required. We adjusted and added *P* and *S* phase arrivals by hand and relocated the events with a generic velocity model (IASP91). Locations were refined using phase picks from as many stations as possible, including CI and land stations not used in the initial detection. Even using the full deployment and land stations, events that occurred early or late in a particular year may suffer from poor coverage, as station siting and recovery spanned several weeks. Events from highly active areas that have

already been characterized in recent studies, like the Nootka fault zone/Vancouver Island north of 48.5°N (Obana et al., 2015) and the Mendocino triple junction region south of 41°N (Chen & McGuire, 2016), were largely excluded from processing during the verification and location steps. Further, catalog completeness drops significantly ~70 km west of the deformation front and ~30 km east of the coastline, corresponding to the aerial distribution of detection stations in a given year.

After the initial location, events with epicenters within or directly adjacent to the CSZ were relocated using Hypoinverse (Klein, 2002). During processing, we employed the same program settings and velocity models used by the PNSN to locate offshore events, providing a means for direct comparison between events recorded by the PNSN and the CI. However, the 1-D velocity models utilized by the PNSN do

Table 1
Event Detection Parameters

Event detection parameters			
Deployment year	STA/LTA	Trigon/Trigoff	T_{min} (s)
Year 1	1/8	3/2	10
Year 2	1/20	4/3	1
Year 3	2/25	4/3	1
Year 4	1/25	4/3	1

Note. "STA/LTA" is the length in seconds of the short-time and long-time moving average windows, "Trigon/Trigoff" describe the ratio of STA/LTA needed to activate and then deactivate a trigger window, and " T_{min} " is the minimum trigger window duration.

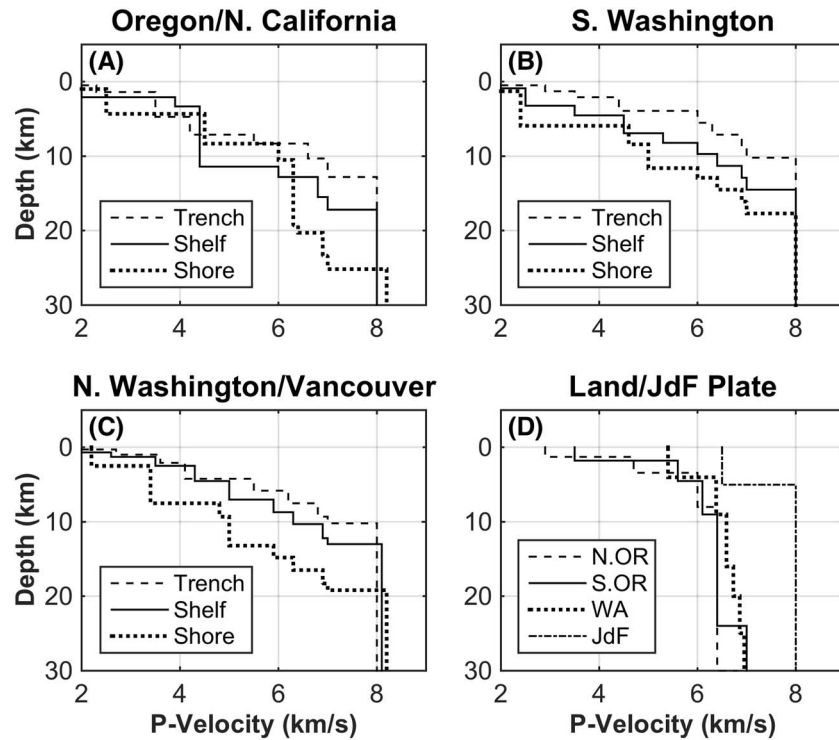


Figure 2. Velocity models used in Hypoinverse for event location. Trench/shelf/shore velocity models were taken from active source seismic experiments (Flueh et al., 1998; Gerdorn et al., 2000). The land/JdF plate velocity models (bottom right plot) are the same as those used by the PNSN in these regions.

not adequately account for the large lateral heterogeneities present in the velocity structure offshore; depending on the location, offshore events were located with a velocity model representing continental crust or the JdF, neither of which reflect the sedimentary mélangé and subducting plate beneath the continental shelf. Further, when iterating to find the event location, the PNSN adopts a relatively liberal phase arrival weighting scheme. Hypoinverse weights phase arrivals relative to the distance between the epicenter and the second -nearest station (dx_2). The PNSN gives nonzero weight to phase arrivals from stations up to 7-times- dx_2 , which is adequate for the land-based network, but is not appropriate for the CI data, where station spacing was sparse and the velocity structure varied significantly over short distances.

To develop velocity models more attuned to the large lateral geologic heterogeneities, we started with the cross sections presented in Flueh et al. (1998) and Gerdorn et al. (2000) developed using active seismic surveys off the coasts of Washington and Oregon. Three 2-D velocity models along lines SO10 and SO12 (Flueh et al., 1998) and profile 7 (Gerdorn et al., 2000) were assigned to their corresponding regions: Northern Washington/Vancouver Island, Southern Washington, and Oregon/Northern California. Within these larger regional designations, we subdivided the area east of the CSZ trench and west of the shore into three 1-D velocity models for input into Hypoinverse; these models correspond to the trench, shelf, and shoreward portions of the subduction zone. Areas outside of the subduction zone (east of the coastline and on the JdF) were assigned the 1-D velocity models in use for those regions by the PNSN. To avoid abrupt transitions crossing from one velocity model to another, we designated 15–25 km buffer zones between adjacent models; the velocity structure in these zones is a linear combination of the neighboring profiles. All velocity profiles are shown in Figure 2, and their corresponding spatial extent in Figure 3. A V_p/V_s ratio of 1.78 was used for all locations, which is the same ratio used by the PNSN. For the phase arrival weighting scheme, we adopted a more conservative distance relation. Phase arrivals within 1.5-times- dx_2 are given full weight, and weights are tapered to zero by 4-times- dx_2 . As such, records from the nearest few stations are given full weight, while enough distant records are retained to reduce azimuthal gaps; very distant records (generally >150–200 km) are not considered.

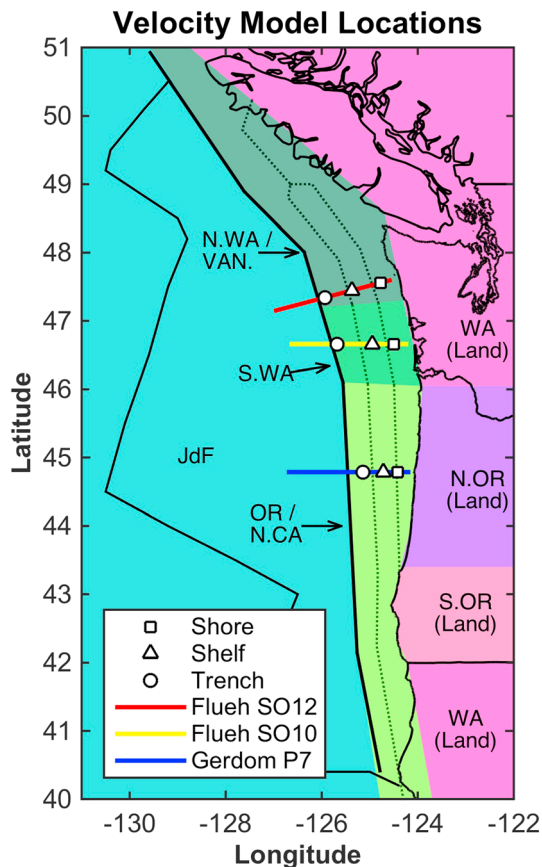


Figure 3. Approximate spatial extent of active source and PNSN velocity models used to locate events near and within the Cascadia subduction zone. The white markers denote the location along the active-source lines where the 1-D models were referenced. The dotted lines denote borders between respective shore, shelf, and trench models. In keeping with the PNSN's protocol, the same velocity model is employed for both landward western Washington and Northern California. Oregon and Northern California (OR/N.CA) correspond to profiles in Figure 2a, southern Washington (S.WA) corresponds to Figure 2b, Northern Washington and Vancouver (N.WA/VAN) correspond to Figure 2c, and land/JdF correspond to Figure 2d.

GR slope between $M_{2.0}$ and 2.5, whereas the central and southern sections have M_c around $M_{1.0}$ –1.5. This particular difference can be partially attributed to the limited extent of the detection stations in the first year, as well as the detection gap off central Washington resulting from noisy, unusable data. While this could affect the observed north-to-south distribution of lower magnitude events ($<M_{2.0}$) and make it difficult to compare along-strike variations in seismicity, it should be noted that when only comparing the number of higher magnitude events ($>M_{2.0}$), the large-scale trends in along-strike seismicity persist. A similar comparison using only the PNSN catalog in the decade preceding the experiment (2006–2016) shows a similar trend, with higher magnitude events increasing in frequency from north to south.

The seismicity observed within the subduction zone can be subset into three major regions based on amount and clustering of activity: north (north of 46°N), central (46°N – 43°N), and south (south of 43°N) (Figure 5). The north region is characterized by very sparse seismicity, with greater event frequency near the coast of Vancouver Island and the Nootka fault zone (Figure 4). Within the central region, activity is associated primarily with the previously identified swarms off Newport, OR, between 44.3°N and 44.7°N (Tréhu et al., 2015), though there is also an active zone of seismicity between 46°N and 45°N . Events in this region are distributed across a wide range of depths, extending from the surface down to the interior of the subducting JdF plate

Magnitudes were determined using a modified version of the local magnitude calculation, wherein a 3–20 Hz, 8-pole band-pass (adj) filter was applied to the data before typical magnitude calculation. This step was added to account for low-frequency noise, which overpowered earthquake signal and skewed magnitude values upward. Filtration parameters were chosen such that events recorded both by the CI and PNSN had similar magnitudes. Average deviation of CI magnitudes from PNSN magnitudes is less than 0.25 magnitude units (see the supporting information for an expanded discussion of our magnitude calculation (Havskov & Ottemoller, 2010; Jennings & Kanamori, 1983; Richter, 1935)).

3. Results

From the 4 years of CI data, we were able to locate 271 earthquakes with epicenters between the Cascadia deformation front and the coastline (Figures 4 and 5). These events have phase arrivals on at least three stations, with a median number of 13 phase arrivals per event. Two example events are shown in Figure 6 with predicted and operator phase picks highlighted. Based on the estimation of Hypoinverse, the median vertical standard error is 1.3 km, and the median horizontal standard error is 2.0 km (Klein, 2002, Appendix 4). Thirty-five events have a vertical standard error greater than 10 km. The majority of these high-uncertainty events are off Northern California and Vancouver Island, which correspond to the regions with the poorest velocity model characterization. The median root-mean-square (RMS) misfit value for the whole data set was 0.46 s. As with location uncertainty, the majority of the 43 events with RMS greater than 1 second occur off Northern California.

The magnitudes of our detected earthquakes range from $M_{0.4}$ to 4.0, with an average uncertainty of $\pm M_{0.48}$ (Figure 7). The cumulative magnitude curves deviate somewhat from a typical Gutenberg-Richter (GR) distribution, both with respect to slope and smoothness, making it difficult to determine a magnitude of completeness (M_c) value. This deviation likely results from large variations in station distribution through the deployment, stringent detection thresholds to account for high noise, and a relatively small catalog size. The northern section of the catalog (north of 46°N) seems to have the highest M_c value, with the slope of the cumulative magnitude curve deviating from a typical

**Detected Near-Shore Earthquake Epicenters
Cascadia Initiative, Years 1-4**

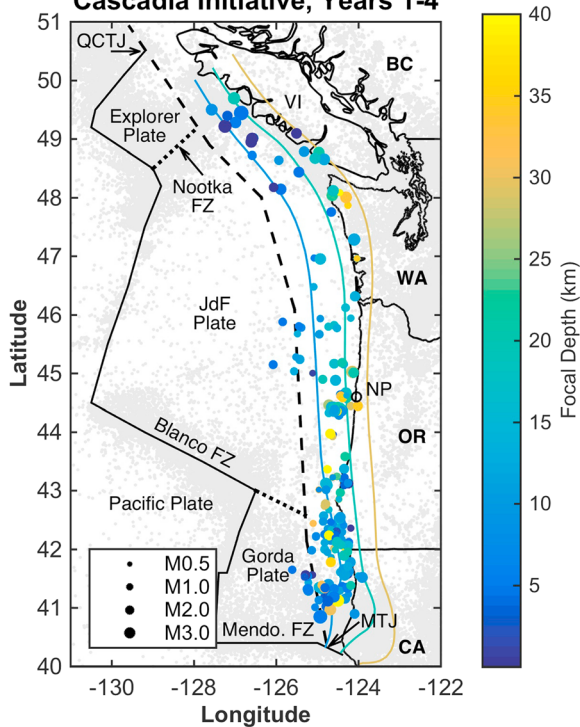


Figure 4. Two hundred seventy-one earthquakes were located with epicenters near the Cascadia subduction zone. The locations shown were calculated in Hypoinverse. Epicenters are color-coded by depth; depth color scale saturates at 40 km to allow comparison of events to plate contours. Contours show depth of the Juan de Fuca plate at 10, 20, and 30 km (McCroly et al., 2012). The grey dots are historical epicenters recorded in land-based catalogs (PNSN, CNSN, and NCSN), with the majority of historical event coming from the 1970–2015 time range. Also labeled on the map are the Queen Charlotte triple junction (QCTJ), the Mendocino triple junction (MTJ), Vancouver Island (VI), and Newport, Oregon (NP, hollow dot shows city location). FZ denotes fault/fracture zone.

CNSN catalogs. Further, the lack of detection stations north of 47°N during the deployment’s first year likely impeded our ability to detect events occurring in the CNSN reporting area.

4. Discussion

Our catalog of offshore seismicity from 41°N to 49°N provides important information about the deformation of the incoming JdF and Gorda plates, as well as the Cascadia fore arc. In the outer rise region of the incoming plates, our data reveal an abrupt transition across 46°N from extremely low seismicity in the north to high seismicity in the south. This trend mirrors seismicity rates observed in the SOSUS (Dziak et al., 2011) and land based catalogs and suggests active deformation south of 46°N (Figure 8). This inference is consistent with structural observations from active source seismic studies (Canales et al., 2017; Gulick et al., 2001; Han et al., 2016, 2017; Horning et al., 2016). During the recent Ridge-to-Trench experiment, small offset normal faults confined to the upper middle crust were imaged in the JdF seaward of the deformation front offshore Washington using multichannel seismic (MCS) reflection data. In contrast, offshore Oregon, large offset normal faults that transect the oceanic crust and extend ~6–7 km into the uppermost mantle were imaged, accompanied by a reduction in V_p in the lower crust (Han et al., 2016; Horning et al., 2016). Coincident MCS and OBS data from an along-strike line just seaward of the deformation front show a transition in crustal reflectivity and lower crustal V_p in the JdF near 45.8°N, suggesting more extensive faulting and a more fractured, hydrated crust offshore Oregon in comparison to Washington (Canales et al., 2017). Offshore of

(Figure 5b). In the southern region, seismicity is abundant and widespread, also spanning a wide range of depths (Figure 5c). While many earthquakes were recorded in the historically active region off Northern California near the Mendocino triple junction, many earthquakes were also observed off southern Oregon and Northern California between 43°N and 41°N as well, including an active swarm at 42.2°N and 124.7°W with ~60 events.

An additional 440 events were located in the incoming plates west of the deformation front (Figure 8). These events were located with only the IASP91 velocity model and are generally associated with higher uncertainty in location. The completeness of this portion of the catalog is strongest within ~70 km of the CSZ, where the events fall within the subset of stations used during event detection. We observe abundant earthquakes along the Blanco fracture zone and some earthquakes associated with the Nootka fault zone. In the outer rise region of the incoming JdF plate, the distribution of earthquakes shows a distinct N-S difference across 46°N (Figure 8). Very few earthquakes are detected offshore Washington, whereas abundant earthquakes are observed south of 46°N offshore Oregon. Offshore Northern California, many earthquakes are detected in the incoming Gorda plate.

During the time of deployment, the PNSN recorded 53 events between the coastline and the deformation front. Of these, 38 were also detected within the CI data; our catalog includes 139 events not detected by the PNSN in its reporting area. Those not detected in the CI data generally occurred during the time of station siting or retrieval or were too weak to be detected on the requisite three stations. Within the NCSN reporting area north of 41°N, 17 events occurred during the deployment, 7 of which were also detected in the CI data; our catalog includes 49 events not detected by the NCSN. In the CNSN catalog south of 49.2°N (south of the Nootka fault zone), 33 events were detected, only 9 of which were detected in the CI data; we located 2 events not detected by the CNSN. It should be noted that detection parameters were initially developed using records from the PNSN catalog, so less emphasis was necessarily given to locating all the events present in the NCSN and

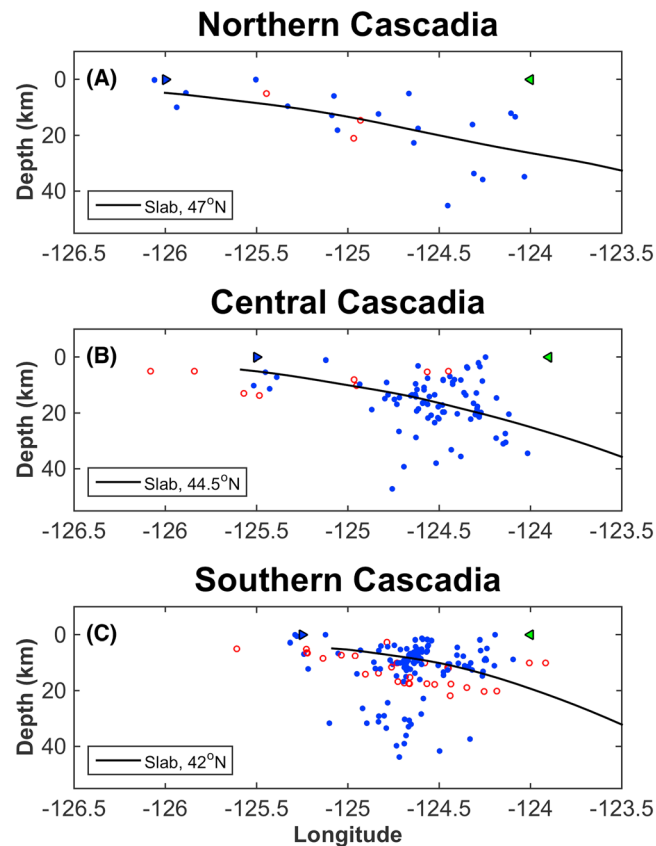


Figure 5. Depths of earthquakes in the (a) north (north of 46°N), (b) central (43°–46°N), and (c) south (south of 43°N) sections of the CSZ. The hollow markers denote events with standard error in depth greater than 10 km, RMS greater than 1 s, or whose depths were fixed by Hypoinverse. The blue triangles denote the location of the deformation front, and the green triangles denote the location of the shoreline. Slab profiles are taken from McCrory et al. (2012). Eleven events west of 126.5°W (off northern Vancouver Island) are not shown.

Northern California, where our catalog documents an even higher rate of seismicity in the incoming Gorda plate, normal faults originally formed near the Gorda ridge are reactivated under north-south compression across the Gorda-Pacific plate boundary as strike-slip faults, causing extensive intraplate deformation (Gulick et al., 2001).

Between the deformation front and the coastline, our catalog shows significant north-south variations in the rate of seismicity at near-plate-interface depths (Figures 4 and 5). If these events are occurring on the plate boundary, this change in seismicity may reflect the locking status and distribution of asperities on the plate interface. Regardless of their source, it seems likely that the change in fore-arc seismicity rates within the CSZ is linked to the along-strike variations in deformation of the incoming plates, as well as to the amount of subducted sediments (Han et al., 2016, 2017; Horning et al., 2016). Both factors affect the roughness/smoothness of the plate interface and the amount of fluid entering the subduction zone, which are important for megathrust slip behavior (Nishikawa & Ide, 2017; Saffer & Tobin, 2011; Wang & Bilek, 2014), as well as the strength and heterogeneity of the subducting slab. In addition, actively deforming strike-slip faults mapped in the overriding North American plate may account for a portion of the increased fore-arc seismicity observed in southern Cascadia (Gulick & Meltzer, 2002).

Here we elaborate on the possible causes of seismicity within the CSZ from north to south. A region-by-region comparison of the influence from underthrust sediments and incoming plate deformation on possible near-plate-interface seismicity is shown in Table 2. In the northern region (north of 46°N), only 33 earthquakes were detected during the OBS deployment period. The relative scarcity of earthquakes on the plate interface offshore Washington mirrors the lack of interface seismicity observed off Vancouver Island during the

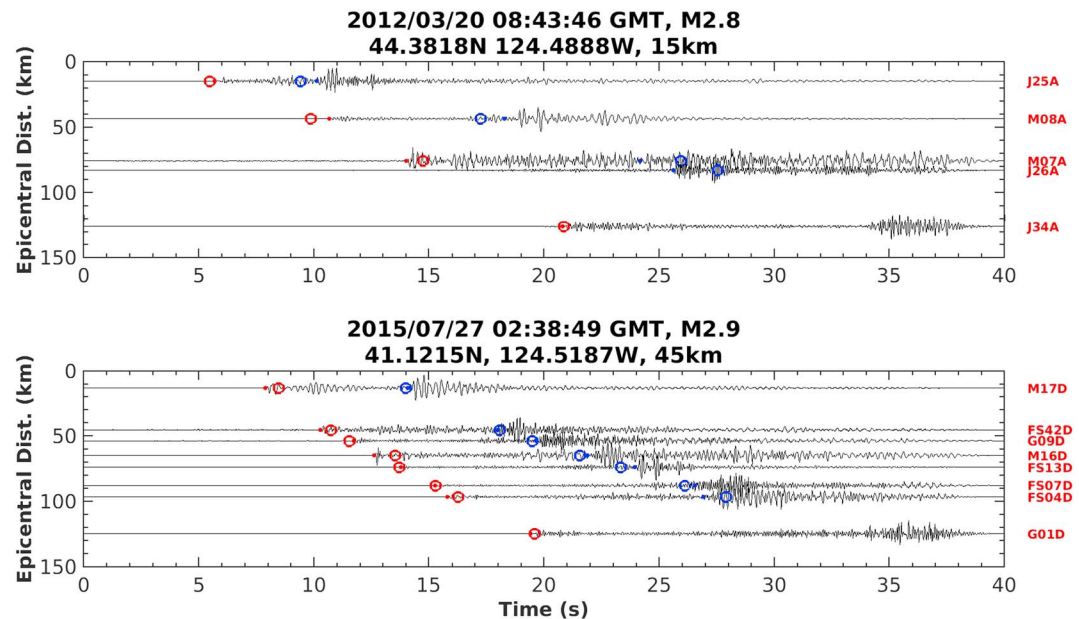


Figure 6. Example seismograms from two events detected in the CI data. Traces shown are vertical channels, with associated CI stations listed to the right. The x axis starts at event origin time; the red and blue dots show operator *P* and *S* phase “hand” picks, respectively; the red and blue circles show *P* and *S* phase arrivals as predicted by Hypoinverse. Titles list event time, magnitude, latitude, longitude, and depth. (top) Event detected during the first year of deployment off the coast of Newport, OR, corresponding to PNSN record 60403911. (bottom) Event detected during the fourth year of deployment off the coast of Northern California, corresponding to NCSN record 72495196.

3 month SeaJade OBS deployment (Obana et al., 2015). This regionally subdued rate of interplate seismicity is consistent with a pervasively locked megathrust north of 46°N, as indicated by land-based geodetic observations (Burgette et al., 2009; McCaffrey et al., 2013; Schmalzle et al., 2014). In this region, the incoming JdF is also less deformed than in its southern portion; the top of the oceanic crust is comparatively smooth with relief less than 150 m (Canales et al., 2017; Han et al., 2016). Overconsolidated sediments are observed near the deformation front and in the outer wedge, with sediments ≤ 600 m thick being subducted (Adam et al., 2004; Booth-Rea et al., 2008; Han et al., 2017). The inferred smooth and fluid-poor interface is favorable for strain accumulation over a larger region.

In the central region (43°N–46°N), many of our detected earthquakes are scattered around the previously identified earthquake clusters between 44.3°N and 44.7°N (Tréhu et al., 2008, 2012, 2015). These clusters have generated several moderately sized earthquakes ($M4+$) in the past with foci near or on the plate interface (Tréhu et al., 2015), and subspace detection of first-year CI time series gathered near the cluster has indicated the presence of active ongoing microseismicity (Morton & Bilek, 2015). Some events from this cluster have been large enough to develop focal mechanisms, most of which show motion characteristic of low-angle thrusting (Tréhu et al., 2012; Williams et al., 2011). Outside of the clusters, the region has had very little observed seismicity. Offshore Central Oregon, partial creeping of the plate interface has been inferred from the land-based geodetic data (Schmalzle et al., 2014). Here a thick sequence (1.4–1.7 km) of underconsolidated sediments are subducting beneath the fore arc (MacKay, 1995; MacKay et al., 1992). The abundant fluid contained in the underthrust sediments along with the permeability structure of the upper plate (Schmalzle et al., 2014) may contribute to the partial creeping of plate interface, which might account for the general lack of seismicity outside of the clusters. Near the earthquake clusters, tomographic, seismic, and magnetic observations indicate the possible presence of a group of subducting seamounts, which could pierce through the sediment sequence and come in contact with the rigid overriding plate (Tréhu et al., 2012; Williams et al., 2011). The earthquakes detected near these clusters in our catalog are distributed over a depth range of ~ 10 km in both the upper plate and lower plate. If this depth distribution is true, it may indicate that as the seamounts subduct, faults and fractures develop in both the upper and lower plates, which generate small earthquakes and create heterogeneous stress on the plate interface (Wang & Bilek, 2014). Between

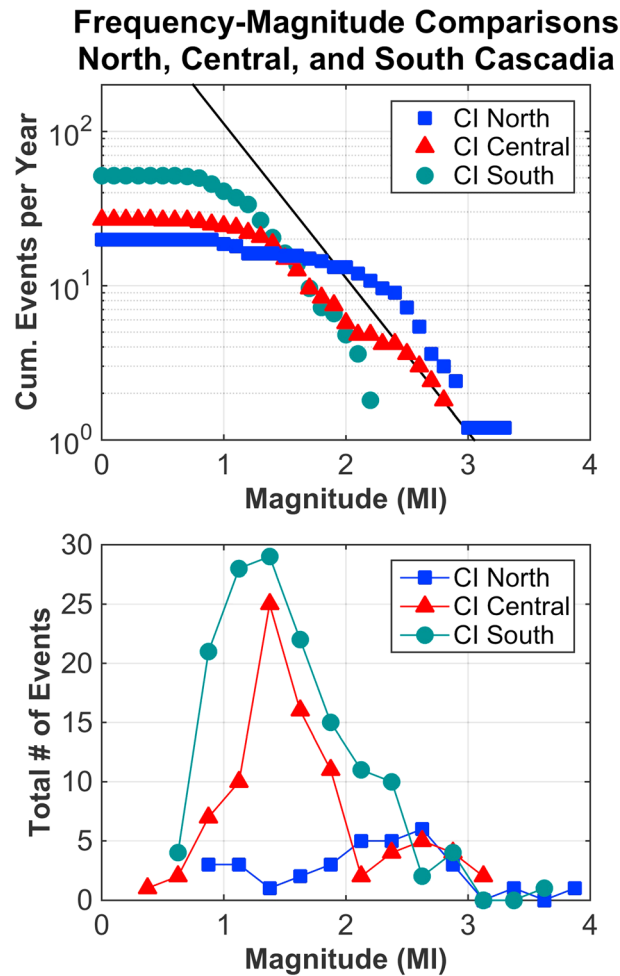


Figure 7. Frequency-magnitude comparisons between the north, central, and south sections of the CSZ as recorded in the CI catalog. (top) Cumulative events per year for each section. The black line has log linear slope of 1. (bottom) Overall number of events per magnitude per section (0.25 magnitude unit binning).

45°N and 46°N, earthquakes are observed over a wide spatial range near the plate interface. With less subducted sediments (≤ 400 m thick) (Booth-Rea et al., 2008; Han et al., 2017; MacKay, 1995) and extensive subduction bending deformation in the oceanic crust, the plate interface in this region may be rougher in comparison to the 43°N–45°N region and has conditions favorable for the generation of small earthquakes.

In the southern region (south of 43°N), abundant earthquakes are detected in the upper plate, near the plate interface, and in the subducting plate. While a high level of seismicity south of 41°N was previously observed from land-based seismic networks, attributed largely to the effect of the Mendocino triple junction on the fore arc and the warping of the slab (McCrory et al., 2012), this is the first time that many small earthquakes have been detected in the expected depth range of the plate interface between 41°N and 43°N. If these events are happening on the plate interface, it may be linked to relatively thin subducted sediments (250–600 m) (Gulick, Meltzer, & Clarke, 1998), and pervasive large-offset faults within the Gorda plate caused by north-south compression (Gulick et al., 2001). The combined effects of these two factors are a relatively rough plate interface and a significantly hydrated oceanic crust. Further, the Blanco fracture zone is subducted near 42.5°N, separating the Gorda plate from the Juan de Fuca plate. This shear zone and two nearby pseudofaults represent major topographic offsets at the basement (Goldfinger et al., 2012) and may locally enhance hydration of the oceanic crust. The associated stress and pore fluid pressure heterogeneities at the plate interface could give rise to small earthquakes in this region.

**Earthquake Epicenters West of Trench
Cascadia Initiative, Years 1-4**

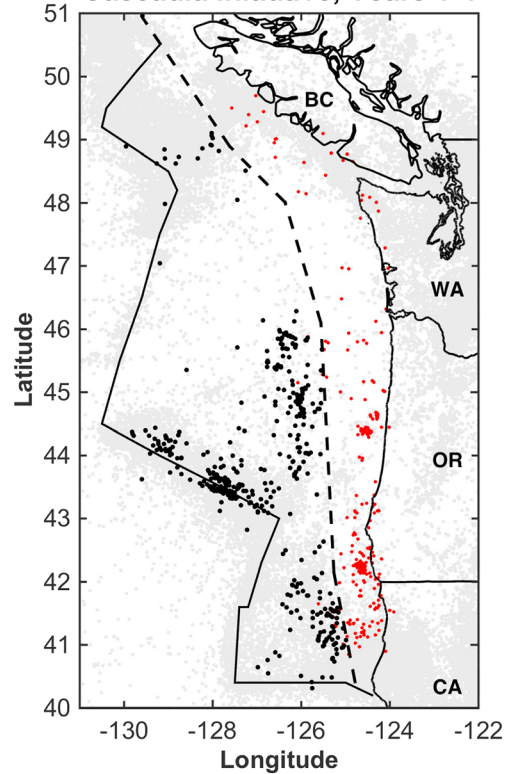


Figure 8. Four hundred forty earthquakes detected to the west of the Cascadia deformation front (black dots) compared to the 271 detected near and adjacent to the megathrust (red dots) and historical land-catalog seismicity (same as in Figure 4, grey dots). Events were located using a generalized IASP91 velocity model.

Shallow, nearshore earthquakes occurring in the southern region’s upper plate fore arc may represent oblique-slip and transpressional faulting. Seismic reflection surveys within the Eel River fore-arc basin just north of the Mendocino triple junction have mapped a number of active faults in the upper plate (Gulick & Meltzer, 2002). These faults may accommodate the incipient northward propagation of the Pacific-North American transform boundary (Gulick & Meltzer, 2002) or relative motion between the northwestern-translating Sierra Nevada-Central Valley microplate and the northern-translating Oregon Coast block

Table 2

Effects of Underthrust Sediment Thickness and Incoming Plate Deformation on Near-Plate-Interface Microseismicity in Each of the Regions Along the Cascadia Subduction Zone

	Underthrust sediments	Deformation of the incoming JdF plate	Resultant degree of hydration	Resultant plate interface smoothness	Microseismicity landward of the deformation front
North Cascadia (north of 46°N)	Thin (≤ 600 m)	Minimal bend-faulting deformation	Less hydrated	Smooth	Very low level of seismicity
Central Cascadia (43°N–46°N)	45°N–46°N: Thin (≤ 500 m)	Largely deformed with deep-cutting faults	More hydrated	45°N–46°N: Rough	45°N–46°N: Relatively high level of seismicity
	43°N–45°N: Thick (1.4–1.7 km)			43°N–45°N: Localized asperities	43°N–45°N: Earthquakes clustered around the inferred subducted seamounts
South Cascadia (south of 43°N)	Thin (250–600 m)	Severely deformed with both bend-faulting and transform deformation	More hydrated	Rough	High level of seismicity

(Unruh & Humphrey, 2017). Additionally, north-south compression from the northward migration of the triple junction has rotated the southernmost portion of the fore arc relative to the rest of the margin, creating an actively faulting transpressional regime at the very southern end of our study area (Gulick & Meltzer, 2002).

5. Conclusions

Using 4 years of CI array data, we locate 271 earthquakes with epicenters between Cascadia's deformation front and the coastline. Little seismicity is observed south of the Nootka fault zone and north of the Washington/Oregon border (49°N–46°N). Off the coast of northern and central Oregon (46°N–43°N), abundant seismicity is observed between 45°N and 46°N and near the previously identified earthquake swarms off Newport, OR (44.3°N–44.7°N). Offshore southern Oregon and Northern California, seismicity is abundant, including a very active swarm off the coast of southern Oregon at 42.2°N and 124.7°W. This distribution of microseismicity illustrates that current near-plate-interface activity within the CSZ is likely related to along-strike variations in subducting plate smoothness and hydration, which are controlled by plate deformation and the thickness of underthrust sediments. Further, abundant upper plate seismicity in the southern portion of the fore arc is likely related to the complex stress field surrounding the Mendocino triple junction. On the incoming plates west of the trench, intraplate seismicity increases significantly south of 46°N. These observations agree with recent active source seismic reflection/refraction studies on the JdF that show more extensive deformation of the subducting plate as the influence of subduction-bending and north-south compression from the Mendocino triple junction increases. While the data from the CI have been invaluable for characterizing present-day seismicity in the CSZ, further robust observations with both temporary and permanent OBS facilities in the subduction zone would likely resolve uncertainties around the origin and distribution of microseismicity, as well as its significance in the larger CSZ seismic cycle.

Acknowledgments

We acknowledge helpful discussion with William Wilcock, as well as suggestions from Sean Gulick and an anonymous reviewer. Thanks to Renate Hartog for help configuring HypoInverse to PNSN settings. Tables containing the 271 subduction zone earthquake locations, the 440 JdF earthquake locations, and 1-D velocity profiles, as well as files containing exact velocity profile locations, are included in the supporting information for this article. Seismograms for this study were obtained from the Data Management Center operated by the Incorporated Research Institutions for Seismology (IRIS). Data analysis was supported by the U.S. National Science Foundation's M9 Hazard SEES grant (EAR-1331412).

References

- Adam, J., Klaeschen, D., Kukowski, N., & Flueh, E. (2004). Upward delamination of Cascadia Basin sediment infill with landward frontal accretion thrusting caused by rapid glacial age material flux. *Tectonics*, *23*, TC3009. <https://doi.org/10.1029/2002TC001475>
- Booth-Rea, G., Klaeschen, D., Grevenmeyer, I., & Reston, T. (2008). Heterogeneous deformation in the Cascadia convergent margin and its relation to thermal gradient (Washington, NW USA). *Tectonics*, *27*, TC4005. <https://doi.org/10.1029/2007TC002209>
- Burgette, R. J., Weldon, R. J., & Schmidt, D. A. (2009). Interseismic uplift rates for western Oregon and along-strike variation in locking on the Cascadia subduction zone. *Journal of Geophysical Research*, *114*, B01408. <https://doi.org/10.1029/2008JB005679>
- Canales, J. P., Carbotte, S. M., Nedimovic, M. R., & Carton, H. (2017). Dry Juan de Fuca slab revealed by quantification of water entering Cascadia subduction zone. *Nature Geoscience*, *10*(11), 864–870. <https://doi.org/10.1038/ngeo3050>
- Chen, X., & McGuire, J. J. (2016). Measuring earthquake source parameters in the Mendocino Triple Junction region using a dense OBS array: Implications for fault strength variations. *Earth and Planetary Science Letters*, *453*, 276–287. <https://doi.org/10.1016/j.epsl.2016.08.022>
- DeMets, C., Gordon, R. G., & Argus, D. F. (2010). Geologically current plate motions. *Geophysical Journal International*, *181*, 1–80. <https://doi.org/10.1111/j.1365-246X.2009.04491.x>
- Dziak, R., Hammond, S., & Fox, C. (2011). A 20-year hydroacoustic time series of seismic and volcanic events in the Northeast Pacific Ocean. *Oceanography*, *24*(3), 280–293. <https://doi.org/10.5670/oceanog.2011.79>
- Flueh, E. R., Fisher, M. A., Bialas, J., Childs, J. R., Klaeschen, D., Kukowski, N., ... Vidal, N. (1998). New seismic images of the Cascadia subduction zone from cruise SO 108-ORWELL. *Tectonophysics*, *293*(1–2), 69–84. [https://doi.org/10.1016/S0040-1951\(98\)00091-2](https://doi.org/10.1016/S0040-1951(98)00091-2)
- Gerdom, M., Tréhu, A. M., Flueh, E. R., & Klaeschen, D. (2000). The continental margin off Oregon from seismic investigations. *Tectonophysics*, *329*(1–4), 79–97. [https://doi.org/10.1016/S0040-1951\(00\)00190-6](https://doi.org/10.1016/S0040-1951(00)00190-6)
- Goldfinger, C., Nelson, C. H., & Johnson, J. E. (2003). Holocene earthquake records from the Cascadia subduction zone and northern San Andreas fault based on precise dating of offshore turbidites. *Annual Review of Earth and Planetary Sciences*, *31*(1), 555–577. <https://doi.org/10.1146/annurev.earth.31.100901.141246>
- Goldfinger, C., Nelson, H. C., Morey, A. E., Johnson, J. E., Patton, J. R., Karabanov, E., ... Vallier, T. (2012). Turbidite event history—Methods and implications for Holocene paleoseismicity of the Cascadia subduction zone: USGS Professional Paper 1661-F. Retrieved from <https://pubs.usgs.gov/pp/pp1661f/>
- Gulick, S. P. S., Meltzer, A. M., & Clarke, S. H. (1998). Seismic structure of the southern Cascadia subduction zone and accretionary prism north of the Mendocino triple junction. *Journal of Geophysical Research*, *103*, 27,207–27,222. <https://doi.org/10.1029/98JB02526>
- Gulick, S. P. S., & Meltzer, A. S. (2002). Effect of the northward-migrating Mendocino triple junction on the Eel River forearc basin, California: Structural evolution. *Bulletin of the Geological Society of America*, *114*(12), 1505–1519. [https://doi.org/10.1130/0016-7606\(2002\)114%3C1505:EOTNMM%3E2.0.CO;2](https://doi.org/10.1130/0016-7606(2002)114%3C1505:EOTNMM%3E2.0.CO;2)
- Gulick, S. P. S., Meltzer, A. S., Henstock, T. J., & Levander, A. (2001). Internal deformation of the southern Gorda plate: Fragmentation of a weak plate near the Mendocino triple junction. *Geology*, *29*(8), 691–694. [https://doi.org/10.1130/0091-7613\(2001\)029%3C0691:IDOTSG%3E2.0.CO;2](https://doi.org/10.1130/0091-7613(2001)029%3C0691:IDOTSG%3E2.0.CO;2)
- Han, S., Bangs, N., Carbotte, S., Saffer, D., & Gibson, J. (2017). Links between sediment consolidation and Cascadia megathrust slip behavior. *Nature Geoscience*, *10*(12), 954–959. <https://doi.org/10.1038/s41561-017-0007-2>
- Han, S., Carbotte, S. M., Canales, J. P., Nedimovic, M. R., Carton, H., Gibson, J. C., & Horning, G. W. (2016). Seismic reflection imaging of the Juan de Fuca plate from ridge to trench: New constraints on the distribution of faulting and evolution of the crust prior to subduction. *Journal of Geophysical Research: Solid Earth*, *121*, 1849–1872. <https://doi.org/10.1002/2015JB012416>
- Havskov, J., & Ottemoller, L. (2010). Magnitudes. In *Routine data processing in earthquake seismology: With sample data, exercises and software* (pp. 151–188). New York: Springer. https://doi.org/10.1007/978-90-481-8697-6_6

- Horning, G., Canales, J. P., Carbotte, S. M., Han, S., Carton, H., Nedimović, M. R., & van Keken, P. E. (2016). A 2-D tomographic model of the Juan de Fuca plate from accretion at axial seamount to subduction at the Cascadia margin from an active source ocean bottom seismometer survey. *Journal of Geophysical Research: Solid Earth*, *121*, 5859–5879. <https://doi.org/10.1002/2016JB013228>
- Hyndman, R. D., Riddihough, R. P., & Herzer, R. (1979). The Nootka Fault Zone—A new plate boundary off western Canada. *Geophysical Journal International*, *58*(3), 667–683. <https://doi.org/10.1111/j.1365-246X.1979.tb04801.x>
- Hyndman, R. D., & Wang, K. (1995). The rupture zone of Cascadia great earthquakes from current deformation and the thermal regime. *Journal of Geophysical Research*, *100*, 22,133–22,154. <https://doi.org/10.1029/95JB01970>
- Jennings, P. C., & Kanamori, H. (1983). Effect of distance on local magnitudes found from strong-motion records. *Bulletin of the Seismological Society of America*, *73*(1), 265–280.
- Klein, F. W. (2002). User's guide to HYPOINVERSE-2000, a Fortran program to solve for earthquake locations and magnitudes: USGS Open File Report 02-171.
- MacKay, M. E. (1995). Structural variation and landward vergence at the toe of the Oregon accretionary prism. *Tectonics*, *14*, 1309–1320. <https://doi.org/10.1029/95TC02320>
- MacKay, M. E., Moore, G. F., Cochrane, G. R., Casey Moore, J., & Kulm, L. V. D. (1992). Landward vergence and oblique structural trends in the Oregon margin accretionary prism: Implications and effect on fluid flow. *Earth and Planetary Science Letters*, *109*(3-4), 477–491. [https://doi.org/10.1016/0012-821X\(92\)90108-8](https://doi.org/10.1016/0012-821X(92)90108-8)
- McCaffrey, R., King, R. W., Payne, S. J., & Lancaster, M. (2013). Active tectonics of northwestern U.S. inferred from GPS-derived surface velocities. *Journal of Geophysical Research: Solid Earth*, *118*, 709–723. <https://doi.org/10.1029/2012JB009473>
- McCroly, P. A., Blair, J. L., Waldhauser, F., & Oppenheimer, D. H. (2012). Juan de Fuca slab geometry and its relation to Wadati-Benioff zone seismicity. *Journal of Geophysical Research*, *117*, B09306. <https://doi.org/10.1029/2012JB009407>
- Morton, E. A., & Bilek, S. L. (2015). Preliminary event detection of earthquakes using the Cascadia Initiative data. *Seismological Research Letters*, *86*(5), 1270–1277. <https://doi.org/10.1785/0220150098>
- Nishikawa, T., & Ide, S. (2017). Detection of earthquake swarms at subduction zones globally : Insights into tectonic controls on swarm activity. *Journal of Geophysical Research: Solid Earth*, *122*, 5325–5343. <https://doi.org/10.1002/2017JB014188>
- Obana, K., Scherwath, M., Yamamoto, Y., Kodaira, S., Wang, K., Spence, G., ... Kao, H. (2015). Earthquake activity in northern Cascadia subduction zone off Vancouver Island revealed by ocean-bottom seismograph observations. *Bulletin of the Seismological Society of America*, *105*(1), 489–495. <https://doi.org/10.1785/0120140095>
- Oppenheimer, D., Beroza, G., Carver, G., Dengler, L., Eaton, J., Gee, L. S., ... Valentine, D. (1993). The Cape Mendocino, California, earthquakes of April 1992—Subduction at the triple junction. *Science*, *261*(5120), 433–438. <https://doi.org/10.1126/science.261.5120.433>
- Richter, C. F. (1935). An instrumental earthquake magnitude scale. *Bulletin of the Seismological Society of America*, *25*(1), 1–32.
- Saffer, D. M., & Tobin, H. J. (2011). Hydrogeology and mechanics of subduction zone Forearcs: Fluid flow and pore pressure. *Annual Review of Earth and Planetary Sciences*, *39*(1), 157–186. <https://doi.org/10.1146/annurev-earth-040610-133408>
- Satake, K., Wang, K., & Atwater, B. F. (2003). Fault slip and seismic moment of the 1700 Cascadia earthquake inferred from Japanese tsunami descriptions. *Journal of Geophysical Research*, *108*(B11), 2535. <https://doi.org/10.1029/2003JB002521>
- Scherwath, M., Spence, G., Obana, K., Kodaira, S., Wang, K., Riedel, M., ... Collins, J. (2011). Seafloor seismometers monitor northern Cascadia earthquakes. *Eos, Transactions of the American Geophysical Union*, *92*(47), 421–422. <https://doi.org/10.1029/2006GL028179>
- Schmalzle, G. M., McCaffrey, R., & Creager, K. C. (2014). Central Cascadia subduction zone creep. *Geochemistry, Geophysics, Geosystems*, *15*, 1515–1532. <https://doi.org/10.1002/2013GC005172>
- Toomey, D. R., Allen, R. M., Barclay, A. H., Bell, S. W., Bromirski, P. D., Carlson, R. L., ... Wilcock, W. S. D. (2014). A sea change in seismological studies of subduction zones. *Oceanography*, *27*(2), 138–150. <https://doi.org/10.5670/oceanog.2014.49>
- Tréhu, A. M., Blakely, R. J., & Williams, M. C. (2012). Subducted seamounts and recent earthquakes beneath the central cascadia forearc. *Geology*, *40*(2), 103–106. <https://doi.org/10.1130/G32460.1>
- Tréhu, A. M., Braunmiller, J., & Davis, E. (2015). Seismicity of the Central Cascadia continental margin near 44.5 N: A decadal view. *Seismological Research Letters*, *86*(3), 819–829. <https://doi.org/10.1785/0220140207>
- Tréhu, A. M., Braunmiller, J., & Nabelek, J. L. (2008). Probable low-angle thrust earthquakes on the Juan de Fuca-North America plate boundary. *Geology*, *36*(2), 127–130. <https://doi.org/10.1130/G24145A.1>
- Unruh, J., & Humphrey, J. (2017). Seismogenic deformation between the Sierran microplate and Oregon Coast block, California, USA. *Geology*, *45*(5), 415–418. <https://doi.org/10.1130/G38696.1>
- Wang, K., & Bilek, S. L. (2014). Invited review paper: Fault creep caused by subduction of rough seafloor relief. *Tectonophysics*, *610*, 1–24. <https://doi.org/10.1016/j.tecto.2013.11.024>
- Wang, K., & Tréhu, A. M. (2016). Invited review paper: Some outstanding issues in the study of great megathrust earthquakes—The Cascadia example. *Journal of Geodynamics*, *98*, 1–18. <https://doi.org/10.1016/j.jog.2016.03.010>
- Williams, M. C., Tréhu, A. M., & Braunmiller, J. (2011). Seismicity at the Cascadia plate boundary beneath the Oregon continental shelf. *Bulletin of the Seismological Society of America*, *101*(3), 940–950. <https://doi.org/10.1785/0120100198>
- Wilson, D. S. (1993). Confidence intervals for motion and deformation of the Juan de Fuca plate. *Journal of Geophysical Research*, *98*, 16,053–16,071. <https://doi.org/10.1029/93JB01227>